Korean J. Chem. Eng., **27**(3), 1003-1009 (2010)
DOI: 10.1007/s11814-010-0154-2

Effect of synthesis condition and annealing on the sensitivity and stability of gas sensors made of Zn-doped γ-Fe_2O_3 particles

Taeyang Kim*,†, Andrew Sharp, and Bing Guo****

*Department of Mechanical Engineering, Korea Military Academy, Seoul, Korea
**Department of Mechanical Engineering, Texas A&M University, College Station, Texas, USA
(*Received 4 October 2009 • accepted 17 November 2009*)

Abstract−Gas sensors made of flame-synthesized Zn-doped γ-Fe_2O_3 nanoparticles were found to have high sensitivity and high aging resistance. Zinc-doped γ-Fe_2O_3 nanoparticles and microparticles were synthesized by flame spray pyrolysis (FSP). Gas sensors were fabricated with as-synthesized particles, and with particles that had been annealed. The sensors' response to acetone vapor and H_2 was measured as fabricated, and measured again after the sensors were aged for three days. The sensors made from as-synthesized particles showed a gas sensing sensitivity 20 times higher than the literature value. However, sensors made of microparticles lost their sensing ability after three days of aging; sensors made of nanoparticles retained their gas sensing capability after aging. Sensors made of annealed particles did not have significant gas sensing capabilities. Analysis using the William and Hall method showed that the microstrains decreased significantly in both H_2/O_2 and H_2/Air flame synthesized particles after annealing. The results showed that sensors made of flame-synthesized particles have much higher sensitivity than sensors made of particles previously reported. Especially, sensors made of flame-synthesized nanoparticles are resistant towards aging. This aging resistance may be attributed to the particles' ability to retain their microstrains.

Key words: Flame Spray Pyrolysis (FSP), Gas Sensing, Sensitivity, Aging, Microstrains

INTRODUCTION

Gas sensors based on semiconductor metal oxides have been one of the most investigated devices to be used as gas sensors. They have aroused the attention of many researchers interested in gas sensing due to their low cost, ease of fabrication, simplicity of use, and large numbers of detectable gases [1]. Their applications range from detection of combustible or toxic gas, to air intake control in automobiles, and to glucose biosensors [2].

Many different metal oxides have been investigated as gas sensor materials. Gamma-iron oxide (γ-Fe_2O_3) is a n-type semiconductor that has attracted research interest due to many merits, such as high sensitivity, low cost, quick response and low power consumption [3]. Tao et al. [4] reported that gas sensitivity of γ-Fe_2O_3 to alcohol was greatly improved by doping Y_2O_3 through a sol-gel process. Jing [5] promoted the sensitivity and selectivity of γ-Fe_2O_3 towards acetone, ethanol, methane, and hydrogen by doping it with Ni. Jiao et al. [6] enhanced the selectivity and stability of gas sensors to acetone, H_2, CO and CH_4 by using SnO_2/Fe_2O_3 multilayer thin film. Yamazoe [7] proposed two types of sensitization mechanism for various dopant materials: chemical sensitization and electronic sensitization.

Flame synthesis is an established commercial process for making inexpensive ceramic nanoparticles (SiO_2, TiO_2: less than $5/kg). Especially, FSP, in which liquid precursors are used, is a promising technique because a broad variety of precursors are available for powder synthesis, although FSP is not yet an established industrial process [8].

†To whom correspondence should be addressed.
E-mail: tykim@kma.ac.kr

Gas sensors should provide long-term performance, even at high operation temperature and in harsh environments. In general, any gas sensing device should exhibit a stable and reproducible signal for the period of at least 2 to 3 years [9]. This requirement means that the stability of a gas sensor is one of the most important factors that determines its practical use.

The conduction mechanisms in metal oxide semiconductor materials are strongly correlated with the intrinsic defect structure. In particular, oxygen vacancies, which are a kind of point defect, are known to behave as donors and have an important role in determining the gas sensing ability [10].

Many parameters affect the stability of a gas sensor, such the grain size of the sensing material (synthesis method), reducing gas, operating temperature, relative humidity, annealing process, film thickness, and deposition method [11]. This study focused on some of these parameters (grain size of sensing material, reducing gas, operating temperature, annealing process) to determine the effect of synthesis conditions and annealing process on the sensitivity and stability of gas sensors made of flame-synthesized Zn-doped γ-Fe_2O_3 particles before and after 3-day aging.

A gamma-Fe_2O_3 based gas sensor detects gases via variations in their resistances. Oxygen electron vacancies in the γ-Fe_2O_3 particles operate as donors, and so provide free charge carriers that transfer oxygen gas to the negatively charged oxygen adsorbates. These playan important role in detecting inflammable gases such as acetone, H_2 and CO. Oxygen adsorbates, such as O^-, are known to cover the surface of semiconductor metal oxides in air, and will eventually dominate the sensor resistance [12].

Sensor selectivity and rate of target gas absorption are influenced by reactions between the sensing material surface and the target gas. These reactions are, in turn, affected by catalysts on the material

surface, ambient conditions, and sensor temperature. When thermal energy is supplied to γ-Fe_2O_3 particles, the free charge carriers (electrons for γ-Fe_2O_3) increase and cause a decrease in resistance. When synthetic air is supplied, the free charge carriers are absorbed by O_2 gas. The surface of γ-Fe_2O_3 acts as an electric potential barrier, which decreases the conduction between particles. Finally, reducing gases are supplied; oxygen adsorbates on the γ-Fe_2O_3 surface are removed by adding reducing gases. This causes the free charge carriers captured in oxygen adsorbates to move into γ-Fe_2O_3 nanoparticles, which weakens the electric potential barrier and increases particle conduction. These processes can be explained by Eqs. (1) and (2).

$$S+e^-+1/2O_2 \leftrightarrow S-O_s^- \quad (1)$$

$$S-O_s^-+R \rightarrow RO+e^-+S \quad (2)$$

Where S denotes a surface adsorption site, e^- is a free electron, R is a reducing gas, such as H_2, CO, C_3H_5O, and S-O_s^- is an oxygen adsorbate. The reversible reaction (1) is affected by temperature and oxygen partial pressure [13].

As a result, the rate of adsorption and desorption of oxygen is a key factor that affects the sensor's sensitivity to various gases.

METHODOLOGY

1. Flame Spray Pyrolysis (FSP) Apparatus

Zn-doped γ-Fe_2O_3 sensor materials were prepared by FSP method using H_2 diffusion flame with O_2 or air support. Fig. 1 shows a schematic of the FSP apparatus. The precursor solution was injected at a steady flow rate (5 ml/hr) into the atomizer vessel by using a syringe pump (Cole Parmer, Vernon Hills, IL). The H_2 fuel gas flowed through the vessel and carried the precursor droplets generated by the atomizer into the flame through the furnace. The droplets underwent solvent evaporation and precursor decomposition to form Zn-doped γ-Fe_2O_3 particles. The H_2 and O_2 (or Air) flow rates were kept at 1 SLM and 6 SLM, respectively. Zn-doped γ-Fe_2O_3 particles then were collected on an alumina filter (Whatman, Maidstone, England). FSP method has been described in detail elsewhere [14].

The precursor solution was prepared by dissolving $Zn(NO_3)_2 \cdot 6H_2O$ (Zinc(III) nitrate hexahydrate, 99.9%, Alfa Aesar) and $Fe(NO_3)_3 \cdot 9H_2O$ (Iron(III) nitrate nonahydrate, 99.9%, Alfa Aesar) in deionized (DI) water. The molar concentration of the solution was 0.75 M (mol/L) in terms of total metal ions, with various Zn/Fe atomic ratios from 0/100 to 100/0.

2. Gas Sensing Apparatus

Zn-doped γ-Fe_2O_3 particles were suspended in DI water. Sonication with an ultrasonic cleaner (VWR International, Arlington, IL) was used to disperse the particles. The DI water suspension of the Fe_2O_3 particles was applied dropwise on the interdigitated electrodes (Case Western Reserve University, Cleveland, OH) to make the gas sensors. Heating the sensor to approximately 150 °C greatly enhanced the speed at which the DI water evaporated, leaving behind a coating of Zn-doped γ-Fe_2O_3 particles. Fig. 2 shows how the gas chamber, picoammeter, power supply, bubbler, and mass flow controller were physically connected throughout the experiments. The gas chamber consisted of an inlet, an outlet, holder for gas sensor and seven signal/power connectors linked to the electrode. First, the initial resistance temperature device (RTD) resistance was measured at room temperature without a gas flow. Eq. (3) is the calibrated resistance to temperature curve for the RTD with an R^2 value of 0.9967.

$$T_{Heater}=56.21*R_{RTD}-241.4 \quad (3)$$

The electrode temperature was controlled by the heater power on the opposite side of the electrode. If at any point the temperature of the electrode fell or rose above the desired temperature, then the power input to the heater was manually adjusted accordingly to maintain the operating conditions.

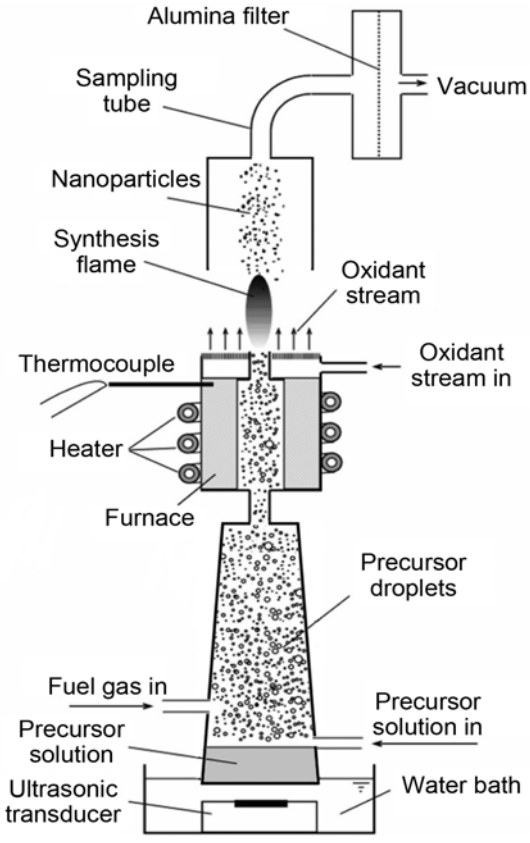

Fig. 1. Schematic of FSP apparatus.

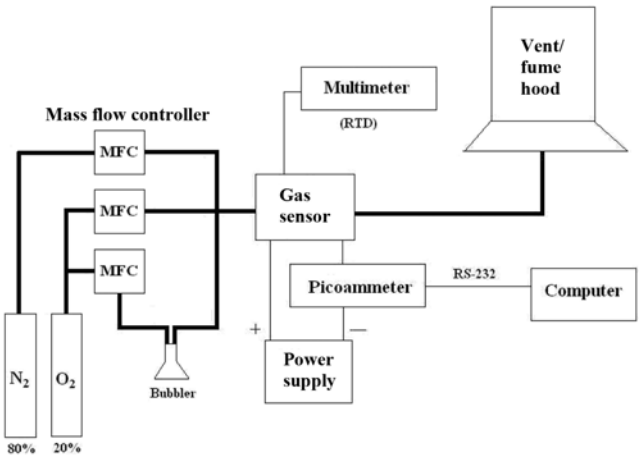

Fig. 2. An illustrative representation of the experimental setup.

Table 1. Flow rates of target gases and synthetic air

Target gas	Acetone vapor				H_2			
Concentration (ppm)	250	500	750	1000	500	1000	1500	2000
Synthetic air (SLM)	4SLM (N_2: 3.2 SLM, O_2: 0.8 SLM)				4SLM (N_2: 3.2 SLM, O_2: 0.8 SLM)			
Flow rate (sccm)	3.6	7.2	10.8	14.5	2	4	6	8

3. Sensor Signal Measurement

Target and background gas flow was controlled by the mass flow controller and their ratio was calculated using partial pressures. Acetone gas was generated by passing oxygen gas through liquid acetone in the bubbler. Measurements during experiments were taken after at least 10 minutes of synthetic air flow only to remove diffusion effects between the sensor material and previous target gas. Synthetic air was used as the background gas to minimize the effect of humidity in the gas. Table 1 displays all the flow rates for background gas and the target gasses corresponding to desired concentration.

Since target gas concentration was a major factor in the rate of adsorption, an accurate method of calculating target gas concentration was required. Using partial pressures and the saturation vapor pressure of the target gas (acetone), the acetone gas was introduced into the main 4 SLM flow of synthetic air via a bubbler. Hydrogen gas was injected into the main 4 SLM flow of synthetic air directly. Synthetic air was used in the experiments to minimize the influence of humidity.

Fig. 3 shows how the connections were created and the quantities measured. Resistance of the RTD was measured using the ohmmeter setting on a multimeter. During the gas sensing experiment, the resistance of the RTD was monitored with an Omega Engineering HHM28 multimeter (OMEGA Engineering, Stamford, CT) to ensure that the gas sensor temperature was constantly within ±5.5 ºC. The picoammeter was connected in series with the sensing material to measure the current across the materials. A voltage of 5.02 V was applied across the sensing material to effectively turn the sensing material into a resistor. Eqs. (4) and (5) show how the current from the picoammeter was converted into the sensor signal. The sensor signal was defined as the ratio of the sensing material's electrical resistance in the background gas, R_b, to the sensing material's electrical resistance in the present of target gas, R_t.

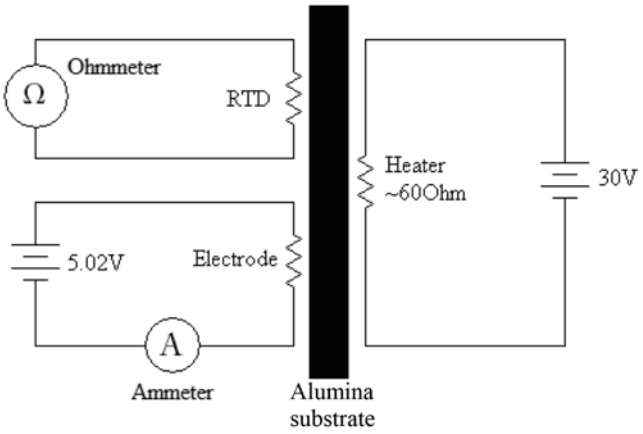

Fig. 3. Illustrative representation of the electrical circuitry.

$$S_{signal}=R_b/R_t \tag{4}$$

$$R_{Material}=\frac{V_{Electrode}}{I_{Picoammeter}}=\frac{5.02\,V}{I_{Picoammeter}} \tag{5}$$

The sensing material's electrical resistance was calculated from the voltage applied on the sensor and the current measured with the picoammeter. The picoammeter read/recorded the current once every two seconds.

4. Sensor Stability Measurement

The stability was defined as the ratio of the signal after aging to the signal before aging.

$$\alpha_{Stability}=S_{after}/S_{before} \tag{6}$$

Several variables affected the stability of gas sensors: synthetic condition, target gas, annealing process. Annealing was performed by leaving Zn-doped γ-Fe_2O_3 particles on a glass plate in the tube furnace for three days, while maintaining existence of ambient air and inside furnace temperature at 325 ºC for H_2/Air flame particles (350 ºC for H_2/O_2 flame) using Thermolyne® 21100 Tube Furnace (Barnstead International, Dubuque, Iowa).

5. Williamson and Hall (WH) Method

The Williamson and Hall (WH) method [12] was used to determine the quantity of microstrain of Zn-doped γ-Fe_2O_3 particles before and after annealing.

Peaks of particles before an after annealing were analyzed with XRD data and the following equations were used for determining the mean microstrain.

$$\beta^*=\beta\cos\theta/\lambda \tag{7}$$

$$d^*=2\sin\theta/\lambda \tag{8}$$

, where β^* is reciprocal peak breadth, β is integral breadth (peak area/maximum intensity), θ is Bragg angle, λ is X-ray wavelength, d* is reciprocal lattice distances. As a result, the mean microstrain of the particles was calculated by plotting β^* versus d* in which the slope of the fitted lines represents the mean microstrain.

RESULTS AND DISCUSSION

1. Particle Size and Morphology

Fig. 4 shows representative TEM images of Zn-doped γ-Fe_2O_3. Particle sizes of Zn-doped γ-Fe_2O_3 formed in H_2/O_2 diffusion flame are much smaller than ones formed in H_2/Air diffusion flame. Adiabatic temperature of H_2/O_2 diffusion flame is about 2,700 ºC and H_2/Air diffusion flame is about 2,100 ºC. That is, high-temperature flame generated nanometer-sized particles; lower temperature flame generated micrometer-sized particles.

This phenomenon can be explained by the melting temperature

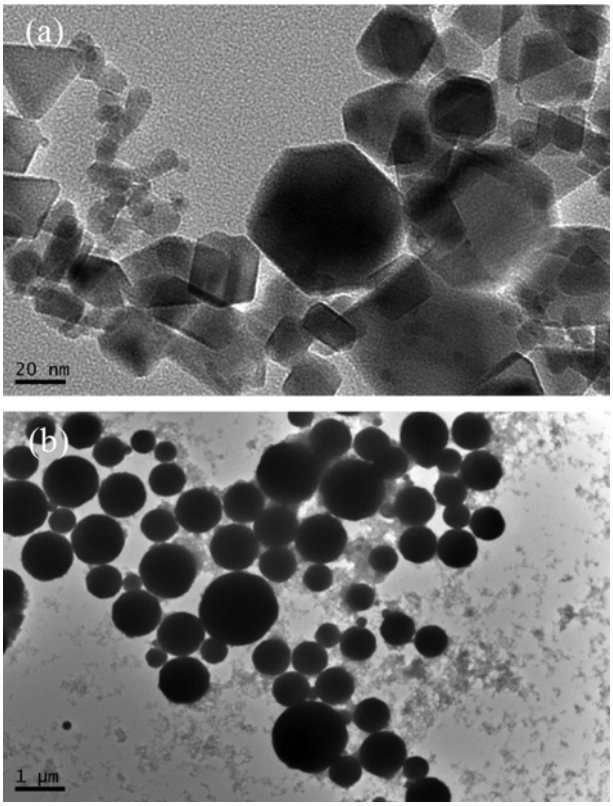

Fig. 4. Representative TEM images of Zn-doped γ-Fe_2O_3 (a) in H_2/O_2 diffusion flame and (b) in H_2/air diffusion flame.

of iron oxide. The melting temperature of iron oxide is 1,566 °C, so iron oxide exists as liquid phase in both flames. However, especially in H_2/O_2 diffusion flame, a larger portion of iron oxide particles would exist in the gas phase than ones formed in H_2/Air diffusion flame. As a result, lower-sized particles are likely to be synthesized in H_2/O_2 diffusion flames.

2. Signal of Gas Sensor

Fig. 5 shows the sensor signals towards acetone of Zn-doped γ-Fe_2O_3 particles synthesized using H_2/Air and H_2/O_2 flames. The two temperatures tested were chosen due to their high signal strength at

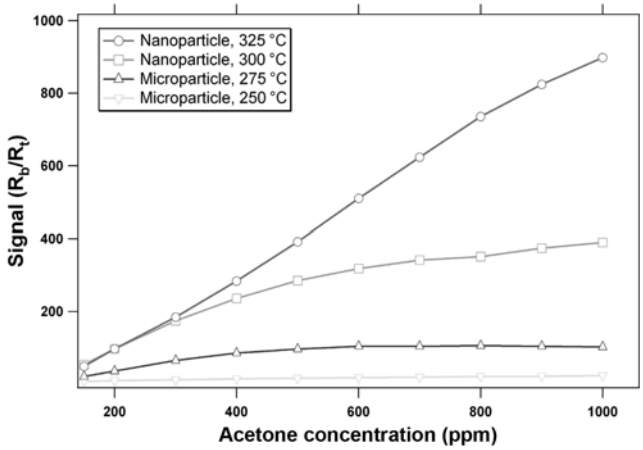

Fig. 5. Signal of γ-Fe_2O_3 gas sensors with various Zn dopant concentrations; to acetone (above) and H_2 gas (below).

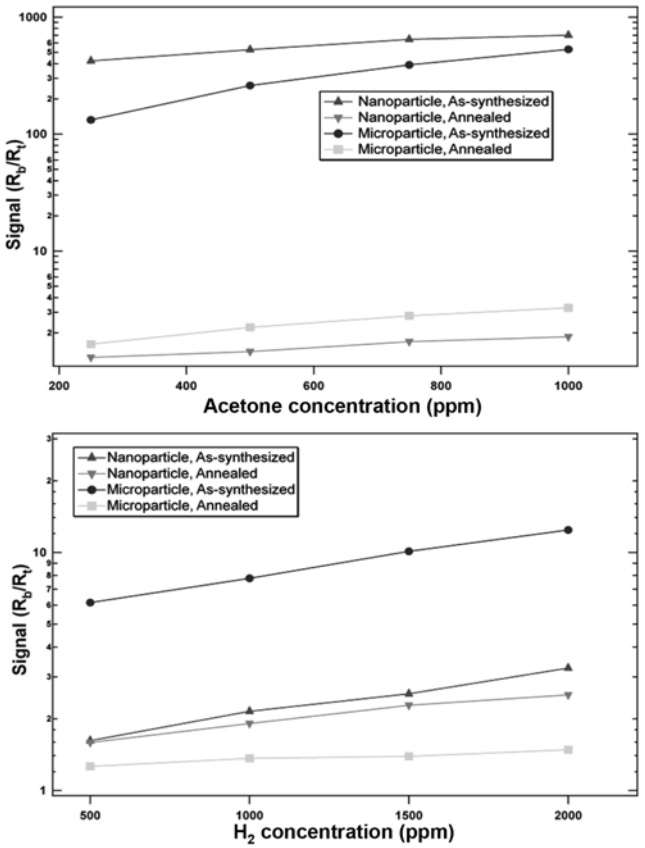

Fig. 6. Signal of sensors made of particles from H_2/O_2 and H_2/air flames as a function of acetone concentrations and sensor temperatures.

1,000 ppm acetone.

The sensors made from nanoparticles showed higher gas sensing sensitivity than sensors made of microparticles, which can be explained by surface area-volume ratio of particles [15]. According to BET measurement, BET surface area of H_2/O_2 flame, as-synthesized particles is 10.4849 m^2/g and BET surface area of H_2/Air flame, as-synthesized particles is 2.8387 m^2/g. The amount of oxygen adsorbates per volume of Zn-doped γ-Fe_2O_3 particles increases with decreasing particle size, causing a further increase in resistance at small particle size [12].

The signals for various target gases and processing methods before and after aging are shown in Figs. 6 and 7. For the sensors made from H_2/O_2 flame, as-synthesized particles showed the highest gas sensing ability. The sensors made of H_2/Air flame particles lost their sensing ability after three days of aging, but sensors made of H_2/O_2 flame particles did not show significant change after aging. However, the sensors made of annealed particles, either micrometer-sized or nanometer-sized, did not show significant gas sensing ability. Tables 2 and 3 display the signals towards 1,000 ppm target gas concentration of sensors made of various particles.

3. TEM Analysis

Fig. 8 shows representative TEM images of Zn-doped γ-Fe_2O_3 made from different synthesis conditions before and after annealing. It proved that the particle size and morphology did not have significant change after annealing process, so that reduction of sensor

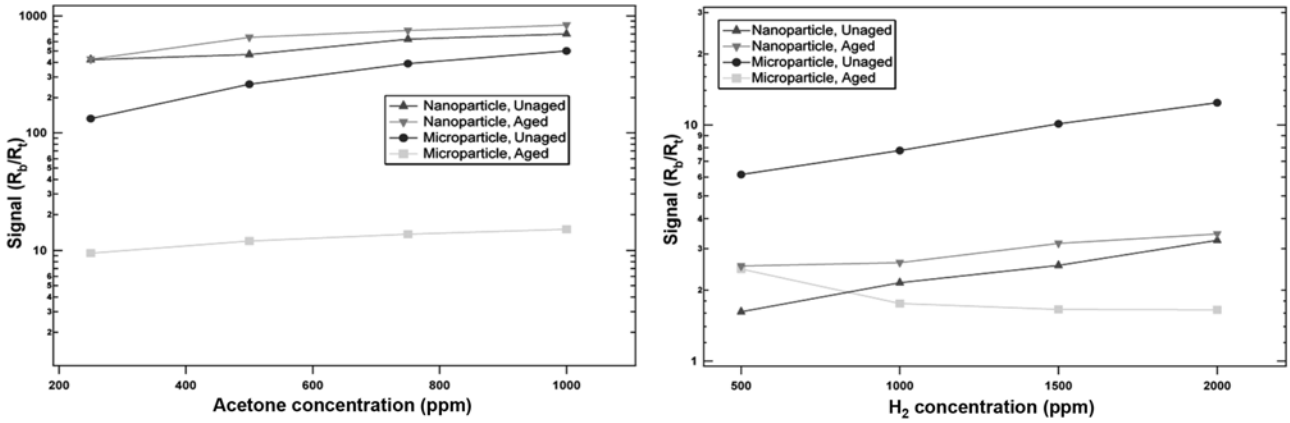

Fig. 7. Signal of gas sensors made of nano and microparticles before and after annealing; to the acetone vapor (above) and H_2 gas (below).

Table 2. Signal of sensors made of various particles towards 1,000 ppm acetone

	H_2/O_2 flame particles		H_2/air flame particles	
	As-synthesized	Annealed	As-synthesized	Annealed
Signal unaged	701.4	3.85	530.9	3.26
Signal aged	831.53	7.1	15.15	2.16

Table 3. Signal of sensors made of various particles towards 1,000 ppm H_2

	H_2/O_2 flame particles		H_2/air flame particles	
	As-synthesized	Annealed	As-synthesized	Annealed
Signal unaged	2.522	3.256	12.41	1.483
Signal aged	3.464	5.427	1.649	1.034

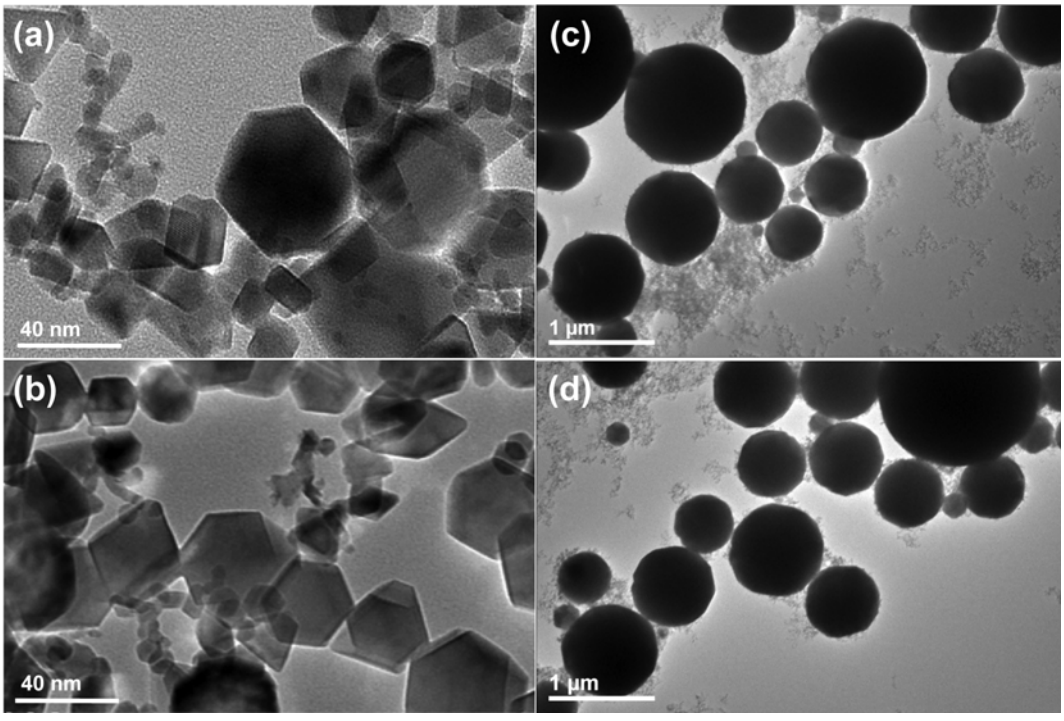

Fig. 8. Signal of gas sensors made of nanoparticles and microparticles before and after aging; to the acetone vapor (above) and H_2 gas (below).

ability after annealing was not because of change of particle size and morphology.

Particle size distributions for different particles are shown in Fig. 9. There was no significant difference in size distribution between the as-synthesized and annealed particles made in both flame. It supported the fact that annealing process did not affect the change

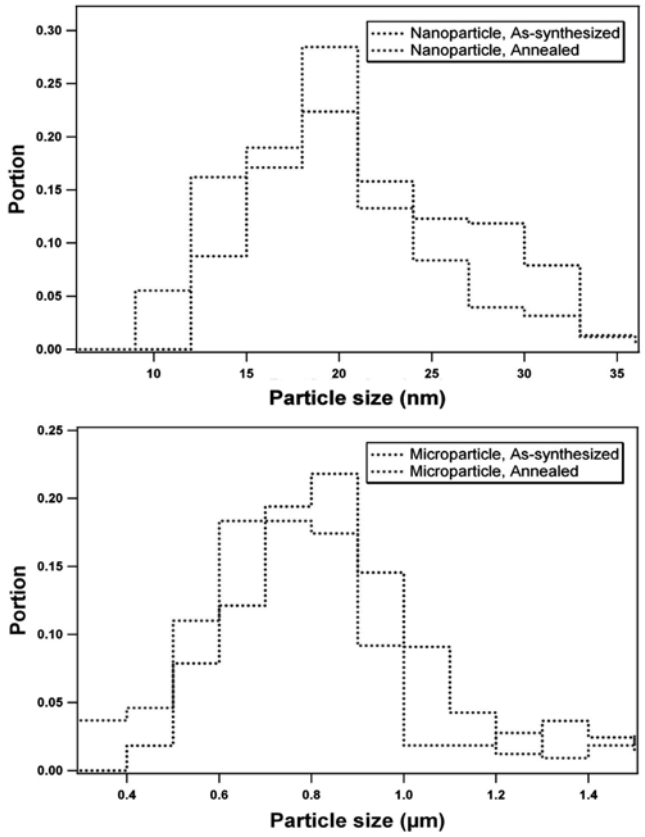

Fig. 9. TEM images of Zn-doped γ-Fe_2O_3; formed in (a) H_2/O_2 diffusion flame, As-synthesized, (b) H_2/O_2 diffusion flame, Annealed, (c) H_2/air diffusion flame, As-synthesized and (d) H_2/Air diffusion flame, Annealed.

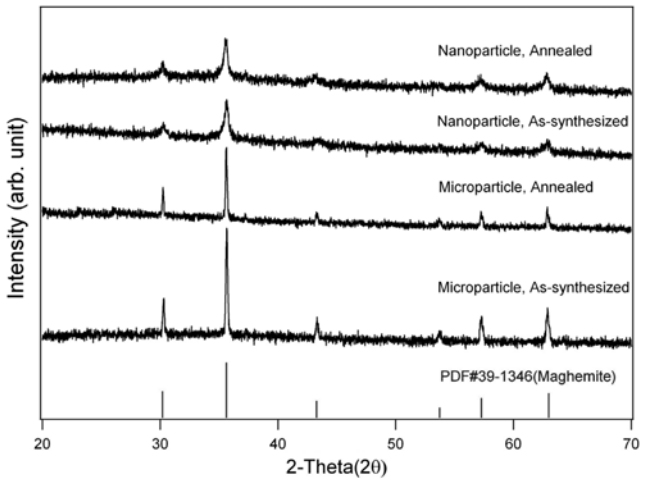

Fig. 10. Particle size distribution for different samples; nanoparticles (above) and microparticles (below).

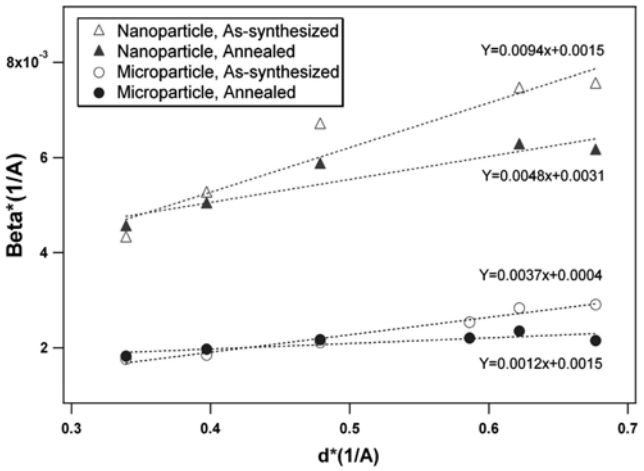

Fig. 11. XRD data for Zn-doped γ-Fe_2O_3 particles made of H_2/air and H_2/O_2 diffusion flames before and after annealing.

of particle size.

4. XRD Analysis

Crystalline structure of Zn-doped γ-Fe_2O_3 particles with various synthesis conditions and processing is shown in Fig. 10; PDF#39-1346 (Maghemite). It indicates that the crystalline structure of Zn-doped γ-Fe_2O_3 particles made of H_2/Air and H_2/O_2 diffusion flames was not changed before or after annealing, so that deterioration of sensor ability after annealing was not because of a change in crystalline structure.

5. Microstrain Analysis: WH Method

Fig. 11 shows the change of mean microstrains of different samples before and after annealing. The slope of the fitted lines decreased two or three times after annealing in H_2/O_2 flame sample, H_2/Air flame sample, respectively. That is, the annealing process had a major effect on improving the lattice quality, reducing point and line defects to a very low level [16].

In conduction mechanisms of metal oxide semiconductors, oxygen vacancies operate as donors, and provide free charge carriers to transfer oxygen gas to negatively charged oxygen adsorbates which play an important role in determining the signal of a gas sensor. An oxygen vacancy is a kind of point defect. Lattice defects, such as dislocations, can either trap or provide extra free electrons [10]. Therefore, we can conclude that one of the possible causes of the reduction in the signal after annealing is associated with the reduction of defects in the Zn-doped Fe_2O_3 layer.

6. Stability of Gas Sensor

The stability of sensors with different processing methods exposed to various target gas concentrations is shown in Fig. 12. In all target gases tested, the sensors made of H_2/O_2 flame particles were more stable than ones made of H_2/Air flame particles. The annealing process was shown to have promoted gas sensor stability. As a result, the synthesis condition using H_2/O_2 diffusion flames and the annealing processing method improved the stability of gas sensors made of flame-synthesized Zn-doped γ-Fe_2O_3 particles.

CONCLUSION

Zn-doped Fe_2O_3 particles synthesized by FSP in a high temperature

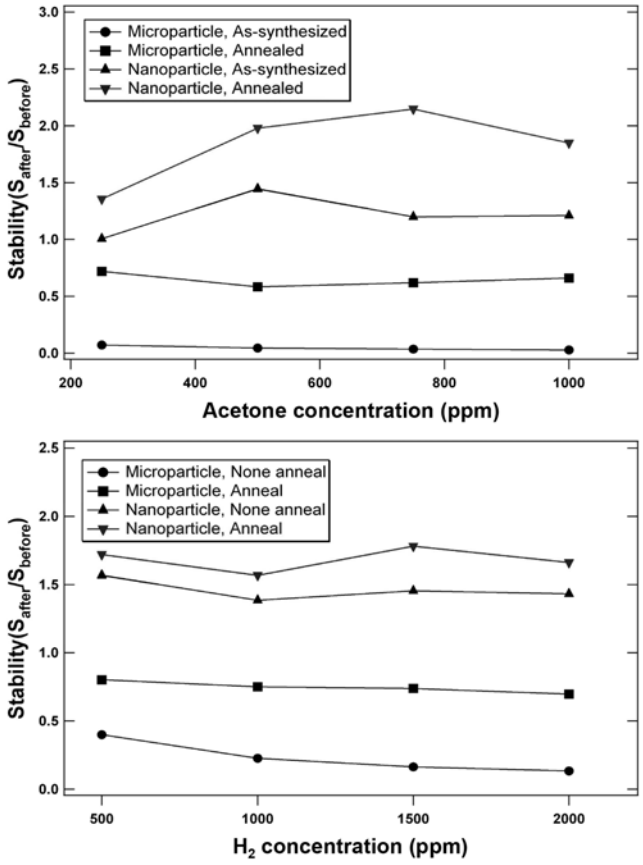

Fig. 12. Stability of gas sensors made of H_2/O_2 and H_2/Air flames, as-synthesized and annealed particles; to the acetone vapor (above) and H_2 gas (below).

flame proved to be more effective in detecting target gases (acetone, H_2 gas) and more resistant towards aging than particles made in a low temperature flame. TEM images showed that high-temperature flames generated nanometer-sized particles. The annealing process decreased the gas sensor's abilities, which can be explained by the WH method analysis. However, the annealing process improved the stability of gas sensors by reducing differences in the signal between the sensor before and after aging. Therefore, the synthesis condition using H_2/O_2 diffusion flames and the annealing process method improved the stability of gas sensors made of flame-synthesized Zn-doped γ-Fe_2O_3 particles.

ACKNOWLEDGMENTS

The author is greatly indebted to faculty members of the Department of Mechanical Engineering in Korea Military Academy for their valuable words of encouragement and advice. And I really appreciate for my wife's devotion that makes me better. Financial support for this research was provided by Texas Engineering Experiment Station and Texas A&M University.

REFERENCES

1. N. Barsan, D. Koziej and U. Weimar, *Sensors and Actuators B-Chemical*, **121**(1), 18 (2007).
2. H. P. Yang and Y. F. Zhu, *Biosensors & Bioelectronics*, **22**(12), 2989 (2007).
3. Z. H. Jing, *Materials Science and Engineering B-Solid State Materials for Advanced Technology*, **133**(1-3), 213 (2006).
4. S. W. Tao, X. Q. Liu, X. F. Chu and Y. S. Shen, *Sensors and Actuators B-Chemical*, **61**(1-3), 33 (1999).
5. Z. H. Jing, *Mater. Lett.*, **60**(28), 3315 (2006).
6. Z. Jiao, S. Y. Wang, L. F. Bian and J. H. Liu, *Mater. Res. Bullet.*, **35**(5), 741 (2000).
7. N. Yamazoe, *Sensors and Actuators B-Chemical*, **5**(1-4), 7 (1991).
8. T. Sahm, L. Madler, A. Gurlo, N. Barsan, S. E. Pratsinis and U. Weimar, *Sensors and Actuators B-Chemical*, **98**(2-3), 148 (2004).
9. G. Korotcenkov, *Materials Science and Engineering B-Solid State Materials for Advanced Technology*, **139**(1), 1 (2007).
10. Z. M. Jarzebski and J. P. Marton, *J. Electrochem. Society*, **123**(7), C199 (1976).
11. M. Graf, A. Gurlo, N. Barsan, U. Weimar and A. Hierlemann, *Journal of Nanoparticle Research*, **8**(6), 823 (2006).
12. Y. Shimizu and M. Egashira, *Mrs Bull.*, **24**(6), 18 (1999).
13. W. Cao, O. K. Tan, W. Zhu, B. Jiang and C. V. G. Reddy, *Sensors and Actuators B-Chemical*, **77**(1-2), 421 (2001).
14. B. Guo and Z. P. Luo, *Journal of the American Ceramic Society*, **91**(5), 1653 (2008).
15. C. Z. Wu, P. Yin, X. Zhu, C. Z. OuYang and Y. Xie, *Journal of Physical Chemistry B.*, **110**(36), 17806 (2006).
16. S. Nicoletti, L. Dori, F. Certicelli, M. Leoni and P. Scardi, *Journal of the American Ceramic Society*, **82**(5), 1201 (1999).